Journal of Materials Chemistry

Cite this: J. Mater. Chem., 2012, 22, 19679

www.rsc.org/materials

PAPER

Synthesis of large-scale undoped and nitrogen-doped amorphous graphene on MgO substrate by chemical vapor deposition†

Jin Zhao,[a] Guoyin Zhu,[a] Wen Huang,[a] Zhi He,[a] Xiaomiao Feng,[a] Yanwen Ma,*[a] Xiaochen Dong,[a] Quli Fan,[a] Lianhui Wang,[a] Zheng Hu,[b] Yinong Lü[c] and Wei Huang*[a]

Received 20th May 2012, Accepted 15th July 2012
DOI: 10.1039/c2jm33209d

Despite amorphous graphene (*a*-graphene) domains having been created and observed within crystalline graphene, large-area synthesis is still in its infancy. Here, using MgO single crystals as a catalytic substrate, large-area (10 × 5 mm) undoped and nitrogen-doped *a*-graphene were synthesized by chemical vapor deposition with benzene and pyridine as precursors, respectively. The dependence of the number of layers and the crystallinity of *a*-graphene on the growth temperature was observed by transmission electron microscopy, selected area electron diffraction and Raman spectroscopy. Few-layer (2–5 layers) *a*-graphene films are demonstrated to have high transmittance (>85% at 550 nm) and low conductivity (<1×10^{-3} S cm^{-1}). When doped with nitrogen (N/C ratio = ~0.09), the conductivity of the *a*-graphene film could be increased. The preparation of large-area *a*-graphene films not only extends to two-dimensional carbon materials but also might provide building blocks for future all-carbon devices.

1. Introduction

Graphene, a crystalline two-dimensional network of sp^2-bonded carbon atoms in a honeycomb lattice, is a semi-metal or zero-gap semiconductor.[1] However, perfect graphene is hard to prepare because crystalline defects always exist.[2–6] The typical stable defects in graphene mainly include mono-vacancies and multi-vacancies, Stone–Wales defects (pentagon–heptagon pairs) and adatoms.[7,8] Polycrystalline graphene containing defects has been demonstrated to have different electronic properties and the controlled engineering of defects allows one to tune its electronic structure at the nanoscale.[5,7] If the defect content significantly increases, *i.e.*, a large amount of sp^2-bonded carbon atoms do not assemble into six rings, amorphous graphene (*a*-graphene) will be generated. Theoretical calculations indicate that *a*-graphene is metallic,[9–12] providing versatile possibilities for engineering graphene electronics. For example, *a*-graphene with tunable resistance has potential applications in flexible and transparent thin film resistors and nanoheaters.

Graphene with small lattice mismatches can be synthesized in large-scale and large-area through chemical vapor deposition (CVD) with the aid of a catalytic metal substrate, such as Ni and Cu foils.[13–16] The growth of graphene on Ni follows the process of carbon dissolution into the bulk, then segregation and/or precipitation on its surface.[17] Graphene grown on Cu is governed by the assembly of catalytically activated carbon atoms on its surface, because the solubility of carbon in Cu is very low, resulting in the predominant formation of single-layer graphene.[15,17] In addition, graphene could also grow on oxides, such as MgO and SiO_2 substrates by free radical condensation (FRC) of hydrocarbons on their surface.[18–21] However, graphene grown on these oxides usually has many more defects than that on metals, which is probably due to the insufficient removal of amorphous carbon in the FRC process. Hence it is possible to increase the graphene crystallization by introducing hydrogen or oxygen during the growth because they are efficient additives for removing amorphous carbon or assisting graphitization.[22–25] This strategy has been well demonstrated by Liu *et al.*[21] in their recent study, *i.e.*, preparing much improved crystalline graphene on SiO_2 or quartz by making use of an oxygen-aided FRC-CVD process. In contrast, without the aid of oxygen as well as using hydrogen-deficient hydrocarbon feed stock, we prepare *a*-graphene on metal oxides. The synthesis of *a*-graphene on oxides not only enriches the two-dimensional carbon structure but also allows the possibility to control their crystallinity if appropriate precursors, oxide substrates or reaction conditions were used. In this paper, undoped and nitrogen-doped amorphous graphene (N-*a*-graphene)

[a]Jiangsu Key Laboratory for Organic Electronics & Information Displays (KLOEID) and Institute of Advanced Materials (IAM), Nanjing University of Posts and Telecommunications, Nanjing 210046, China. E-mail: iamwhuang@njupt.edu.cn; iamywma@njupt.edu.cn; Fax: +86 25 8349 2333; Tel: +86 25 8586 6008
[b]Key Laboratory of Mesoscopic Chemistry of MOE and Jiangsu Provincial Lab for Nanotechnology, School of Chemistry and Chemical Engineering, Nanjing University, Nanjing, 210093, China
[c]College of Materials Science and Engineering, Nanjing University of Technology, Nanjing 210009, China

† Electronic supplementary information (ESI) available: SEM images of *a*-graphene films, AFM images of *a*-graphene films, TEM image and SAED pattern of N-*a*-G-700 film, Nitrogen content of N-*a*-graphene films measured by XPS and plots of conductivity as a function of transmittance. See DOI: 10.1039/c2jm33209d

were grown on an MgO (100) single crystalline substrate from benzene and pyridine, respectively, by CVD at ambient pressure. Moreover, simply adjusting the reaction temperature allows us to facilely change the number of layers. The single- or few-layer *a*-graphene and N-*a*-graphene sheets are transparent and exhibit typical electrical resistance characteristics.

2. Experimental

2.1. Synthesis of *a*-graphene on MgO substrate

A double-side polished single crystal (100) oriented MgO substrate (10 × 5 × 0.5 mm) was placed in the center of a quartz tube mounted inside a horizontal tube furnace. The furnace was heated at a rate of 10 °C min^{-1} in Ar to the preset reaction temperature. Then 0.25 ml of benzene was injected into the reactor at a rate of 12.5 μl min^{-1} and carried to the surface of the MgO substrate by Ar gas with a flow of 40 sccm. After reaction for 20 min, the furnace was naturally cooled to room temperature under Ar gas protection. The *a*-graphene synthesized at 650, 700, 750 and 800 °C were denoted as *a*-G-650, *a*-G-700, *a*-G-750 and *a*-G-800, respectively. N-*a*-graphene films were synthesized by a similar process using pyridine as a precursor and were denoted as N-*a*-G-650, N-*a*-G-700, N-*a*-G-750 and N-*a*-G-800, according to the reaction temperature.

2.2. Transferral of *a*-graphene onto SiO_2–Si substrate

The transferral of *a*-graphene onto SiO_2–Si substrate (200 nm thermal oxide) was carried out similar to the method for graphene grown on a metal substrate.[26] The *a*-graphene film was protected by polymethylmethacrylate (PMMA) and released from the MgO substrate by etching the substrate in HCl (1 M) solution. After washing with deionized water three times, the PMMA/*a*-graphene film was transferred to the SiO_2–Si substrate and was dried at 85 °C for 5 min. Finally, the PMMA film was dissolved in acetone, leaving the *a*-graphene on the SiO_2–Si substrate.

2.3. Characterization

Undoped and N-doped *a*-graphene were characterized by optical microscopy (Olympus BX51), scanning electron microscopy (SEM, Hitachi S-4800), transmission electron microscopy (TEM, JEM2010 at 200 kV with point resolution of 0.19 nm), X-ray photoelectron spectroscopy (XPS, PHI5000 VersaProbe), and Raman spectroscopy (Renishaw inVia Raman Microscope with an argon-ion laser at an excitation wavelength of 514 nm). The transmittance of *a*-graphene was calculated from that of *a*-graphene–MgO, which was carried out using an ultraviolet–visible spectrometer (UV-3600, Shimadzu) with the calibration of a bare MgO substrate. The electrical properties of the *a*-graphene film were measured using a two-point probe *I*–*V* station (Keithley 2400 semiconductor parameter) at room temperature. The gold electrodes with a channel length of 100 μm and a channel width of 2000 μm were thermally evaporated onto the *a*-graphene–MgO films. The obtained current–voltage (*I*–*V*) curves were used to calculate the conductivity.

3. Results and discussion

The digital photographs of the *a*-graphene and N-*a*-graphene films on MgO substrates are shown in Fig. 1a and b, respectively. It is clearly seen that the transparency of the films dropped gradually with increasing deposition temperature from 650 to 800 °C, indicating their continuous growth in thickness. Among them, the N-*a*-G-800 (the abbreviation manner is given in the Experimental section) has the lowest visual transparency, *i.e.*, the highest thickness. When the graphene film is transferred onto the SiO_2–Si substrate, its contrast with the optical micrograph could be used to identify its profile, as well as evaluating its thickness.[27] From the color regularity and the contrast evolution of the films in Fig. 1c–f, it is learnt that the *a*-graphene films keep their large-area integration well after transportation and their thicknesses increase with increasing reaction temperature. The SEM observation gives a consistent result (Fig. S1 in ESI†). The N-*a*-graphene films in Fig. 1g–j present similar phenomena and trends. The results suggest that large-area graphene-like film can be grown on a single crystal MgO surface.

Fig. 2a and b show the transmission electron microscopy (TEM) images of *a*-G-750 and N-*a*-G-750. The sheets have typical graphene features. They are transparent and crumpled and spread on lacy carbon TEM grids, which indicates that the sheets are flexible. The chemical compositions of the *a*-graphene and N-*a*-graphene films were analyzed by XPS and the spectra of the *a*-G-750 and N-*a*-G-750 on SiO_2–Si substrates are representatively given in Fig. 2c. The survey scan spectra show the C1s, O1s, Si2s and Si2p signals for each film as well as an additional N1s peak for the N-*a*-graphene film. The Si signals definitely come from the SiO_2–Si substrates while the O1s peak originates from the SiO_2 substrate with possible contributions of oxygen species on the graphene. The calculated nitrogen to carbon atomic ratio for each N-*a*-graphene film is in the range of 0.085–0.096 (Table S1 in ESI†). The N1s spectrum for N-*a*-G-750 (Fig. 2d) can be fitted to three N entities, including pyridinic N, pyrrolic N and graphitic N with binding energies of 398.8, 400.2 and 401.4 eV, respectively.[28] The amount of graphitic N is

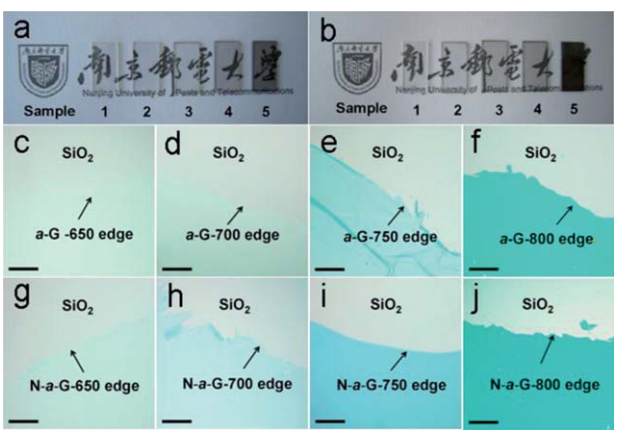

Fig. 1 Digital photographs of *a*-graphene (a) and N-*a*-graphene films on MgO substrates (b). (1) Bare MgO substrate, (2)–(5) the films prepared at 650, 700, 750 and 800 °C, respectively. Optical micrographs of *a*-graphene (c–f) and N-*a*-graphene films on SiO_2–Si substrates (g–j). Scale bar is 30 μm.

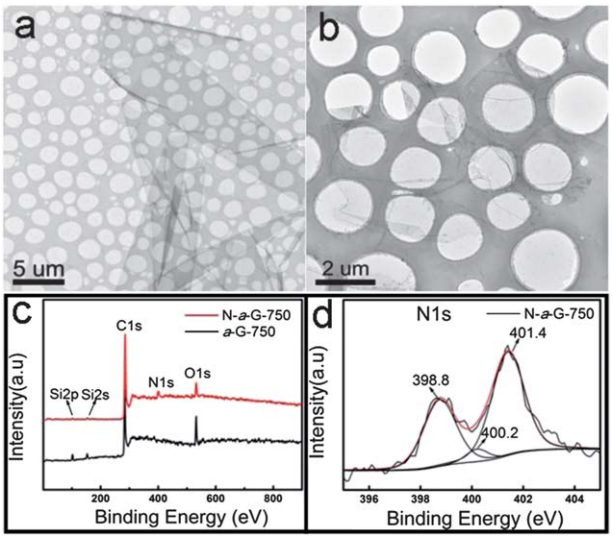

Fig. 2 TEM images of *a*-G-750 (a) and N-*a*-G-750 (b); (c) survey XPS spectra of *a*-G-750 and N-*a*-G-750 films on SiO_2–Si substrates. (d) N 1s narrow scan spectrum of N-*a*-G-750.

larger than that of pyridinic N, which indicates that considerable numbers of pyridine molecules were broken down. Hence the graphene lattice is predominantly assembled by the cracked C and N species rather than C_5N six-membered rings.[28]

The microstructures of the *a*-graphene films were investigated by TEM and are given in Fig. 3. From the edge of each sample, it is seen that the *a*-G-650, *a*-G-700, *a*-G-750 and *a*-G-800 have layers of 1–2, 2–3, 4–5 and 12–14, respectively. The results are consistent with the atomic force microscopy (AFM) measurements (Fig. S2 in ESI†). In addition, the stacking order of the graphene sheets was improved with increasing reaction temperature, which means

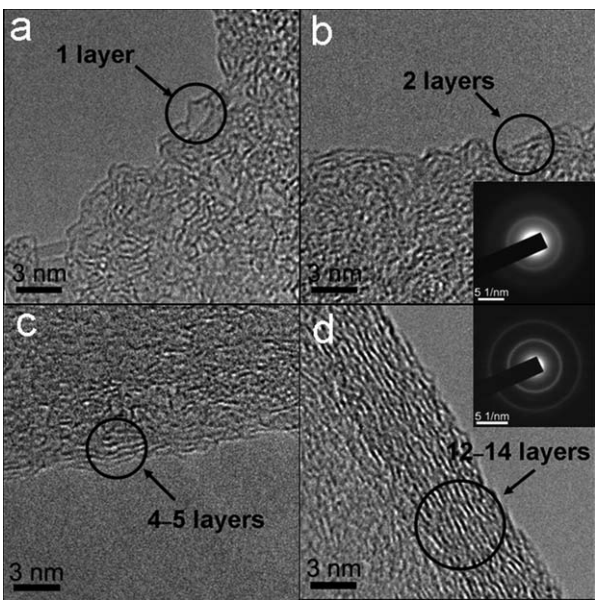

Fig. 3 TEM images of *a*-G-650 (a), *a*-G-700 (b), *a*-G-750 (c) and *a*-G-800 films (d). The insets in (b) and (d) are the SAED patterns of the *a*-G-700 and *a*-G-800 films, respectively.

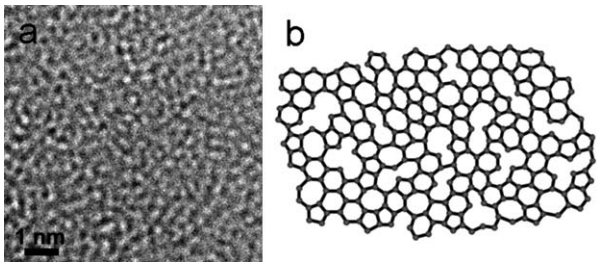

Fig. 4 (a) HRTEM images of the *a*-G-650 film. (b) Schematic diagram of the *a*-graphene.

the enhancement of graphitization. A similar changing tendency for the number of layers and the crystallinity with reaction temperature was also observed in the growth of carbon nanocages on MgO particles, where the crystallinity was qualitatively evaluated by the oxidation temperature using thermogravimetry.[29] In this case, the selected area electron diffraction (SAED) patterns of *a*-G-700 and *a*-G-800 are given to illustrate this evolution. The SAED pattern of *a*-G-700 (inset in Fig. 3b) is a halo ring, which is indicative of amorphous carbon. The crystallinity of *a*-G-800 was improved, leading to two clearer diffraction rings appearing in the SAED pattern (inset in Fig. 3d). But it still belongs to disordered or amorphous graphene as reflected by the inexistence of diffraction dots. The high-resolution TEM image of *a*-G-650 film is shown in Fig. 4a, in which the regular lattice fringe could not be observed, while many dark spots related to vacancy sites appear. This further reveals that the obtained graphene is amorphous. The possible atom structure of the *a*-graphene is depicted by the schematic diagram (Fig. 4b). The disordered lattice of the *a*-graphene is filled with Stone–Wales defects, polygonal rings, point or even line defects. The growth of *a*-graphene rather than a single-crystal structure on the MgO substrate indicates that the C6-rings of the benzene molecules are broken during the reaction.[28] At 700 °C, the obtained N-doped *a*-graphene, *i.e.*, N-*a*-G-700 has 3–4 layer sheets, a little more than *a*-G-700. Moreover, the N-*a*-G-700 shows a more diffusive ring in its SAED pattern than the *a*-G-700, indicating the higher amorphization due to nitrogen doping (Fig. S3 in ESI†).

Raman spectroscopy is a sensitive tool for the structural characterization of graphene, and there are several reports about Raman measurements on defects in graphene.[30–34] Fig. 5 shows the Raman spectra of the undoped (Fig. 5a) and N-doped *a*-graphene (Fig. 5b) together with the derived intensity ratios of the D band to G band (I_D/I_G, Fig. 5c), as well as the evolution of the G peak positions (Fig. 5d). Unlike the spectrum of single- or polycrystalline graphene which have a pronounced 2D peak near ~2700 cm^{-1}, those of the undoped and N-doped graphene exhibit significantly depressed and broaden 2D peaks. The vanishing of the 2D band for the graphene sheet should result from the amorphization, which is evidenced by the *a*-graphene resulting from the bombardment of low-energy argon ions.[32,33] As observed from Fig. 5c, the values of I_D/I_G for the *a*-graphene films are in the range of 0.71–0.86 and the linewidth of the G peaks are about 150 cm^{-1}. Ferrari and Schwan *et al.* have proposed an extrapolation method to evaluate the size of the sp^2 graphitic cluster in amorphous carbon from its I_D/I_G and G peak position.[35,36] Making use of this method, we deduced that the

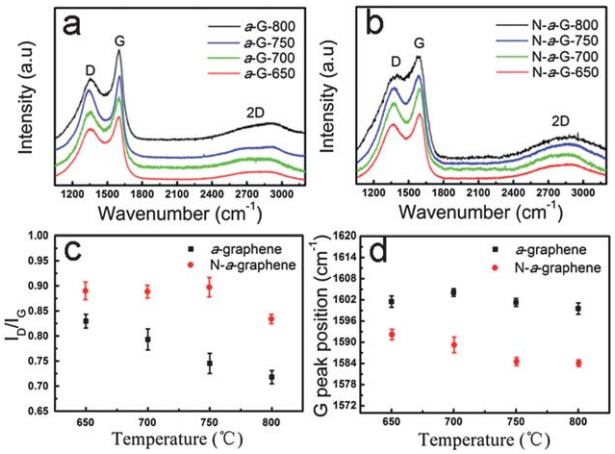

Fig. 5 Raman spectra of *a*-graphene (a) and N-*a*-graphene films on the Si–SiO_2 substrate (b). (c) I_D/I_G *vs.* reaction temperature. (d) G peak position *vs.* reaction temperature.

ordered graphene domain size in our *a*-graphene sheet is smaller than 1 nm. The values of I_D/I_G for the N-doped *a*-graphene films are 0.87–0.93, much higher than those for the undoped ones, indicating that the N-doped *a*-graphene films have much higher disorder, in accordance with the SAED results. The G peak dispersion for each specimen is given in Fig. 5d. It is known that the G peak position of graphene is not only affected by the defect amount,[33] but also by the number of layers.[37] High disorder will upshift the G peak over 1600 cm^{-1}, while a layer increase downshifts it to within ~6 cm^{-1}. In this case, the G peak of each *a*-graphene film is located at a higher wavenumber of 1590–1604 cm^{-1} with respect to that of highly-crystalline graphene (~1585 cm^{-1}). Specifically, these G peaks undergo a downshift at the higher reaction temperature (750 and 800 °C) due to the simultaneous increase of graphitization and layer number. As for the N-doped *a*-graphene films, their G peak positions also present significant downshift dispersion due to the additional contributions from nitrogen doping.[38] According to the amorphization trajectory proposed by Ferrari and Robertson,[39] we deduced that the obtained *a*-graphene films are composed of predominantly sp^2 carbon and a small amount of sp^3 carbon (2–12%). Hence, the Raman results further support that the graphene films grown on the MgO substrate are amorphous.

Fig. 6 shows the transmittance spectra of the undoped and N-doped *a*-graphene films on the MgO substrates, which were characterized by UV-vis spectroscopy. As can be seen, the transmittance of the *a*-graphene and the N-doped *a*-graphene films decrease with the growth temperature because of the increase of the number of layers (Fig. 3). The transmittance at 550 nm for each specimen is listed in the figures. In comparison to the graphene grown on Cu that has the same number of layers (~95% for 2-layer graphene),[40] the *a*-graphene grown on MgO has a lower transmittance. This is perhaps due to some impurities attached onto the surface of the *a*-graphene films.

To evaluate the electrical properties of the as prepared *a*-graphene films, we have fabricated diodes directly on graphene–MgO films with Au as electrode; the channel length and width are 100 and 2000 μm, respectively. Fig. 7a and b show the current–voltage (*I*–*V*) characteristics of the undoped and N-doped

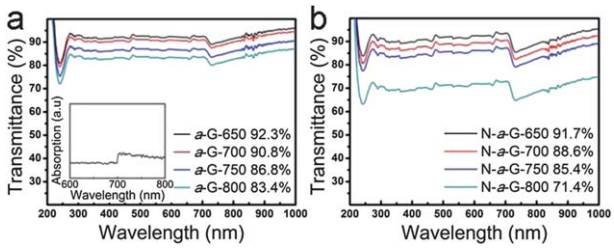

Fig. 6 Transmittance spectra of *a*-graphene (a) and N-doped *a*-graphene films (b). The data listed in the figures are the transmittance of the films at $\lambda = 550$ nm. The inset in (a) is the absorption spectrum of the bare MgO substrate that has an adsorption peak at 700 nm.

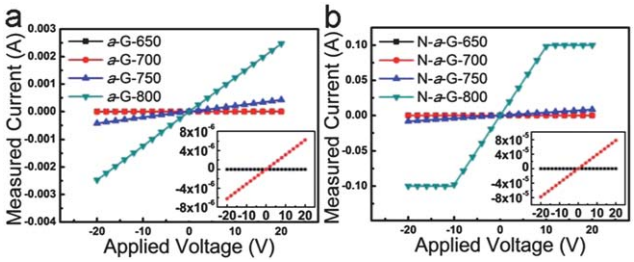

Fig. 7 *I*–*V* characteristics of undoped *a*-graphene films (a) and N-doped *a*-graphene films (b). The current of N-*a*-G-800 overruns the preset value under a high forward voltage (>~10 V) or reverse voltage (<~−10 V).

a-graphene films, respectively. As expected, our *a*-graphene films offer linear *I*–*V* characteristics of a typical metallic material in the voltage range of −20 to 20 V. However, the *a*-G-650 and N-*a*-G-650 show the electrical behavior of insulator, probably due to their discontinuous growth on MgO. It is calculated that the conductivities of *a*-G-700, *a*-G-750 and *a*-G-800 are 3.1×10^{-5}, 2.1×10^{-3} and 0.12 S cm^{-1}, respectively. These conductivities are remarkably smaller than that of graphene grown on Cu or Ni by six to ten orders of magnitude. The conductivities of N-*a*-G-700, N-*a*-G-750 and N-*a*-G-800 are calculated to be 3.9×10^{-4}, 4.2×10^{-2} and 0.98 S cm^{-1}, respectively, which are higher than those of the undoped ones according to the plot of conductivity as a function of transmittance (Fig. S4 in ESI†). This may be attributed to the additional electrons provided by nitrogen doping. Hence, the resistance of *a*-graphene could be tuned by variation of the number of layers, graphitization and nitrogen doping, which is expected to be used for high electrical resistance for future all-carbon electronics.

4. Conclusions

A method has been developed to prepare large-scale undoped and N-doped *a*-graphene on an MgO single crystalline substrate using a CVD process where the precursors are benzene and pyridine, respectively. The number of *a*-graphene layers could be roughly tuned in the range of 1–14 layers by varying the growth temperature. Accordingly, its transmittance at $\lambda = 550$ nm changes from 92% to 83%. These *a*-graphene films are a type of high electrical resistance materials and the lowest conductivity of *a*-G-700 can reach 3×10^{-5} S cm^{-1}. Nitrogen doping could remarkably improve the conductivity of *a*-graphene, providing an alternative way to modulate its electrical properties. It is

expected that *a*-graphene may give rise to some intriguing electrical, optical and mechanical properties, as well as being useful in future graphene-based devices.

Acknowledgements

This work is jointly supported by the National Basic Research Program of China (2009CB930600, 2012CB933301), the Ministry of Education of China (No. IRT1148), A Project Funded by the Priority Academic Program Development of Jiangsu Higher Education Institutions, NSFC (20833002, 20903057, 20905038, 20974046), Key Projects for International Cooperation (BZ2010043), RFDP (20093223120002), and Jiangsu Provincial NSF (BK2010525, BK2011750).

Notes and references

1 K. S. Novoselov, A. K. Geim, S. V. Morozov, D. Jiang, Y. Zhang, S. V. Dubonos, I. V. Grigorieva and A. A. Firsov, *Science*, 2004, **306**, 666–669.
2 H. Ayako, S. Kazu, G. Alexandre, U. Koki and I. Sumio, *Nature*, 2004, **430**, 870–873.
3 M. H. Gass, U. Bangert, A. L. Bleloch, P. Wang, R. R. Nair and A. K. Geim, *Nat. Nanotechnol.*, 2008, **3**, 676–681.
4 P. Y. Huang, C. S. Ruiz-Vargas, A. M. van der Zande, W. S. Whitney, M. P. Levendorf, J. W. Kevek, S. Garg, J. S. Alden, C. J. Hustedt, Y. Zhu, J. Park, P. L. McEuen and D. A. Muller, *Nature*, 2011, **469**, 389–393.
5 J. Lahiri, Y. Lin, P. Bozkurt, I. I. Oleynik and M. Batzill, *Nat. Nanotechnol.*, 2010, **5**, 326–329.
6 K. Erickson, R. Erni, Z. Lee, N. Alem, W. Gannett and A. Zettl, *Adv. Mater.*, 2010, **22**, 4467–4472.
7 O. V. Yazyev and S. G. Louie, *Nat. Mater.*, 2010, **6**, 806–809.
8 F. Banhart, J. Kotakoski and A. V. Krasheninnikov, *ACS Nano*, 2011, **5**, 26–41.
9 V. Kapko, D. A. Drabold and M. F. Thorpe, *Phys. Status Solidi B*, 2010, **247**, 1197–1200.
10 J. Kotakoski, A. V. Krasheninnikov, U. Kaiser and J. C. Meyer, *Phys. Rev. Lett.*, 2011, **106**, 105505.
11 E. Holmström, J. Fransson, O. Eriksson, R. Lizárraga, B. Sanyal, S. Bhandary and M. I. Katsnelson, *Phys. Rev. B: Condens. Matter Mater. Phys.*, 2011, **84**, 205414.
12 Y. Li, F. Inam, A. Kumar, M. F. Thorpe and D. A. Drabold, *Phys. Status Solidi B*, 2011, **248**, 2082–2086.
13 A. Reina, X. Jia, J. Ho, D. Nezich, H. Son, V. Bulovic, M. S. Dresselhaus and J. Kong, *Nano Lett.*, 2009, **9**, 30–35.
14 K. S. Kim, Y. Zhao, H. Jang, S. Y. Lee, J. M. Kim, K. S. Kim, J. H. Ahn, P. Kim, J. Y. Choi and B. H. Hong, *Nature*, 2009, **457**, 706–710.
15 X. Li, W. Cai, J. H. An, S. Kim, J. Nah, D. Yang, R. Piner, A. Velamakanni, I. Jung, E. Tutuc, S. K. Banerjee, L. Colombo and R. S. Ruoff, *Science*, 2009, **324**, 1312–1314.
16 L. G. D. Arco, Y. Zhang, A. Kumar and C. Zhou, *IEEE Trans. Nanotechnol.*, 2009, **8**, 135–138.
17 X. Li, W. Cai, L. Colombo and R. S. Ruoff, *Nano Lett.*, 2009, **9**, 4268–4272.
18 M. H. Rümmeli, A. Bachmatiuk, A. Scott, F. Börrnert, J. H. Warner, V. Hoffman, J.-H. Lin, G. Cuniberti and B. Büchner, *ACS Nano*, 2010, **4**, 4206–4210.
19 S. Gaddam, C. Bjelkevig, S. Ge, K. Fukutani, P. A. Dowben and J. A. Kelber, *J. Phys.: Condens. Matter*, 2011, **23**, 072204.
20 L. Kong, C. Bjelkevig, S. Gaddam, M. Zhou, Y. H. Lee, G. H. Han, H. K. Jeong, N. Wu, Z. Zhang, J. Xiao, P. A. Dowben and J. A. Kelber, *J. Phys. Chem. C*, 2010, **114**, 21618–21624.
21 J. Chen, Y. Wen, Y. Guo, B. Wu, L. Huang, Y. Xue, D. Geng, D. Wang, G. Yu and Y. Liu, *J. Am. Chem. Soc.*, 2011, **133**, 17548–17551.
22 M. Glerup, H. Kanzow, R. Almairac, M. Castignolles and P. Bernier, *Chem. Phys. Lett.*, 2003, **377**, 293–298.
23 H. J. Park, J. Meyer, S. Roth and V. Skákalová, *Carbon*, 2010, **48**, 1008–1094.
24 M. H. Rümmeli, C. Kramberger, A. Grüneis, P. Ayala, T. Gemming, B. Büchner and T. Pichler, *Chem. Mater.*, 2007, **19**, 4016–4017.
25 M. H. Rümmeli, F. Schäffel, C. Kramberger, T. Gemming, A. Bachmatiuk, R. J. Kalenczuk, B. Rellinghaus, B. Büchner and T. Pichler, *J. Am. Chem. Soc.*, 2007, **129**, 15772–15773.
26 A. Reina, H. Son, L. Jiao, B. Fan, M. S. Dresselhaus, Z. Liu and J. Kong, *J. Phys. Chem. C*, 2008, **112**, 17741–17744.
27 P. Blake, E. W. Hill, A. H. C. Neto, K. S. Novoselov, D. Jiang, R. Yang, T. J. Booth and A. K. Geim, *Appl. Phys. Lett.*, 2007, **91**, 063124.
28 H. Chen, Y. Yang, Z. Hu, K. F. Huo, Y. W. Ma, Y. Chen, X. S. Wang and Y. N. Lu, *J. Phys. Chem. B*, 2006, **110**, 16422–16427.
29 K. Xie, X. T. Qin, X. Z. Wang, Y. N. Wang, H. S. Tao, Q. Wu, L. J. Yang and Z. Hu, *Adv. Mater.*, 2012, **24**, 347–352.
30 A. C. Ferrari, *Solid State Commun.*, 2007, **143**, 47–57.
31 C. Casiraghi, A. Hartschuh, H. Qian, S. Piscanec, C. Georgi, A. Fasoli, K. S. Novoselov, D. M. Basko and A. C. Ferrari, *Nano Lett.*, 2009, **9**, 1433–1441.
32 M. M. Lucchese, F. Stavale, E. H. Martins Ferreira, C. Vilani, M. V. O. Moutinho, R. B. Capaz, C. A. Achete and A. Jorio, *Carbon*, 2010, **48**, 1592–1597.
33 L. G. Cançado, A. Jorio, E. H. Martins Ferreira, F. Stavale, C. A. Achete, R. B. Capaz, M. V. O. Moutinho, A. Lombardo, T. Kulmala and A. C. Ferrari, *Nano Lett.*, 2011, **11**, 3190–3196.
34 E. H. Martins Ferreira, M. V. O. Moutinho, F. Stavale, M. M. Lucchese, R. B. Capaz, C. A. Achete and A. Jorio, *Phys. Rev. B: Condens. Matter Mater. Phys.*, 2010, **82**, 125492.
35 A. C. Ferrari, S. E. Rodil and J. Robertson, *Phys. Rev. B: Condens. Matter*, 2003, **67**, 155306.
36 J. Schwan, S. Ulrich, V. Batori, H. Ehrhardt and S. R. P. Silva, *J. Appl. Phys.*, 1996, **80**, 440–447.
37 A. Gupta, G. Chen, P. Joshi, S. Tadigadapa and P. C. Eklund, *Nano Lett.*, 2006, **6**, 2667–2673.
38 D. Wei, Y. Liu, Y. Wang, H. Zhang, L. Huang and G. Yu, *Nano Lett.*, 2009, **9**, 1752–1758.
39 A. C. Ferrari and J. Robertson, *Philos. Trans. R. Soc. London, Ser. A*, 2004, **362**, 2477–2512.
40 X. Li, Y. Zhu, W. Cai, M. Borysiak, B. Han, D. Chen, R. D. Piner, L. Colombo and R. S. Ruoff, *Nano Lett.*, 2009, **9**, 4359–4363.